Study of Nanoscale Morphology of Polythiophene Fibrils and Fullerene Derivative.

ARTICLE *in* ACS APPLIED MATERIALS & INTERFACES · JULY 2014

Impact Factor: 6.72 · DOI: 10.1021/am502577s · Source: PubMed

5 AUTHORS, INCLUDING:

Nopporn Rujisamphan
King Mongkut's University of Technology Tho…
12 PUBLICATIONS **69** CITATIONS
SEE PROFILE

Roy Murray
National Institute of Standards and Technology
17 PUBLICATIONS **33** CITATIONS
SEE PROFILE

Fei Deng
University of Delaware
19 PUBLICATIONS **167** CITATIONS
SEE PROFILE

Syed Ismat Shah
University of Delaware
265 PUBLICATIONS **4,369** CITATIONS
SEE PROFILE

ACS APPLIED MATERIALS & INTERFACES

Research Article

www.acsami.org

Study of the Nanoscale Morphology of Polythiophene Fibrils and a Fullerene Derivative

Nopporn Rujisamphan,[†] Roy E. Murray,[‡] Fei Deng,[†] Chaoying Ni,[†] and S. Ismat Shah*[,†,‡]

[†]Department of Materials Science and Engineering and [‡]Department of Physics and Astronomy, University of Delaware, Newark, Delaware 19716, United States

Supporting Information

ABSTRACT: Nanoscale blending of electron-donor and electron-acceptor materials in solution-processed bulk heterojunction organic photovoltaic devices is crucial for achieving high power conversion efficiency. We used a classic blend of poly(3-hexylthiophene)/phenyl-C_{61}-butyric acid methyl ester (P3HT/PCBM) as a model to observe the nanoscale morphology of the P3HT fibrils and PCBM nanoclusters in the mixture. Energy-filtered transmission electron microscopy (EFTEM) clearly revealed a nanoscopic phase separation. Randomly connected and/or nonconnected P3HT fibrous networks and PCBM domains, revealed by 2-dimensional micrographs, were observed by collecting electron energy loss spectra in the range of 19−30 eV. From EFTEM images, the average length and the diameter of P3HT fibrils were found to be approximately 70 ± 5 and 15 ± 2 nm, respectively. Combining the EFTEM, selected area electron diffraction, and X-ray diffraction results, the number and spacing of the ordered chains in P3HT fibrils were determined. There were 18 ± 3 repeating units of P3HT perpendicular to the fibril, ∼184 layers of $\pi-\pi$ stacking along the fibril, and ∼9 layers of interchain stacking within the fibril. These conclusive observations provide insight into the number of molecules found in one instance of ordered-plane stacking. This information is useful for the calculation of charge transport in semicrystalline polymers. Using cross-section samples prepared with a focused ion beam technique, the vertical morphology of each phase was analyzed. By collecting 30 eV energy loss images, the phase separation in the P3HT/PCBM system was distinguishable. A higher P3HT concentration was observed at the top of the cell, near Al contact, which could possibly cause loss of carriers and recombination due to a mismatch in the P3HT and Al energy bands.

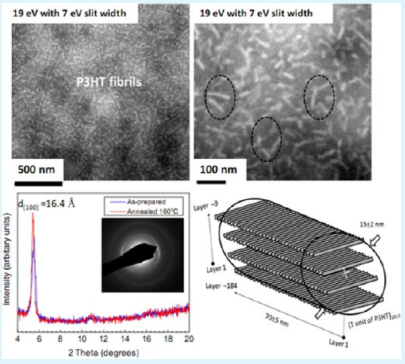

KEYWORDS: *organic photovoltaic, P3HT fibril, energy-filtered TEM, electron energy loss spectroscopy*

1. INTRODUCTION

A rapid increase in the power conversion efficiency (PCE) of organic photovoltaic (OPV) devices, particularly with bulk heterojunction (BHJ) architecture, is an indication of its potential for economical device production and an alternative route toward renewable energy.[1,2] In traditional BHJ systems, the active layer is fabricated in such a way that interfacial contact areas are maximized by controlling the ratio of an electron-donating polymer and an electron-accepting molecule, usually a fullerene derivative. The PCE of BHJ systems reached 9.2% recently (in a mixture of thieno[3,4-*b*]thiophene/benzodithiophene (PTB7) and [6,6]-phenyl-C_{71}-butyric acid methyl ester ($PC_{71}BM$)), as reported by He et al.[3] It is also well understood that, in OPV devices, exciton separation occurs as it reaches the interface between donor and acceptor domains.[4,5] Once these excitons are separated, charge transport must occur to carry the electrons and holes toward the respective electrodes. This transport is hindered by the low mobility that is typical of most organic materials, poly(3-hexylthiophene) (P3HT) and phenyl-C_{61}-butyric acid methyl ester (PCBM) included. The hole mobility of P3HT was reported to be on the order of $10^{-4}-10^{-5}$ cm^2 V^{-1} s^{-1}.[6,7] Moreover, charge transport routes calculated with molecular dynamic (MD) simulations by Lan et al.[8,9] showed that the most significant charge hopping route in the P3HT fibrils is along the intrachain direction. Work by Kevin et al.[10] also showed that infiltration of the P3HT polymer into the nanopores of an anodic alumina template results in the enhancement of hole mobility by a factor of 20.

It has been accepted that a well-controlled BHJ morphology with an interdigitated structure[11] consisting of a nanoscale bipercolation pathway corresponding to the exciton diffusion length is highly desired to achieve high device performance. Ruderer et al.[12] and Guo et al.[13] illustrated that a lateral-phase morphology and vertical-phase composition had profound impacts on device characteristics and performance. Combining topographies from atomic force microscopy (AFM), X-ray reflectivity (XRR), and grazing incidence wide-angle X-ray scattering (GISAXS) characterizations allowed the authors to be able to draw the vertical-phase morphology across the sample's thickness. Gaining a better understanding of the nanoscale morphology, including the fibril structure, will

Received: December 17, 2013
Accepted: July 23, 2014
Published: July 23, 2014

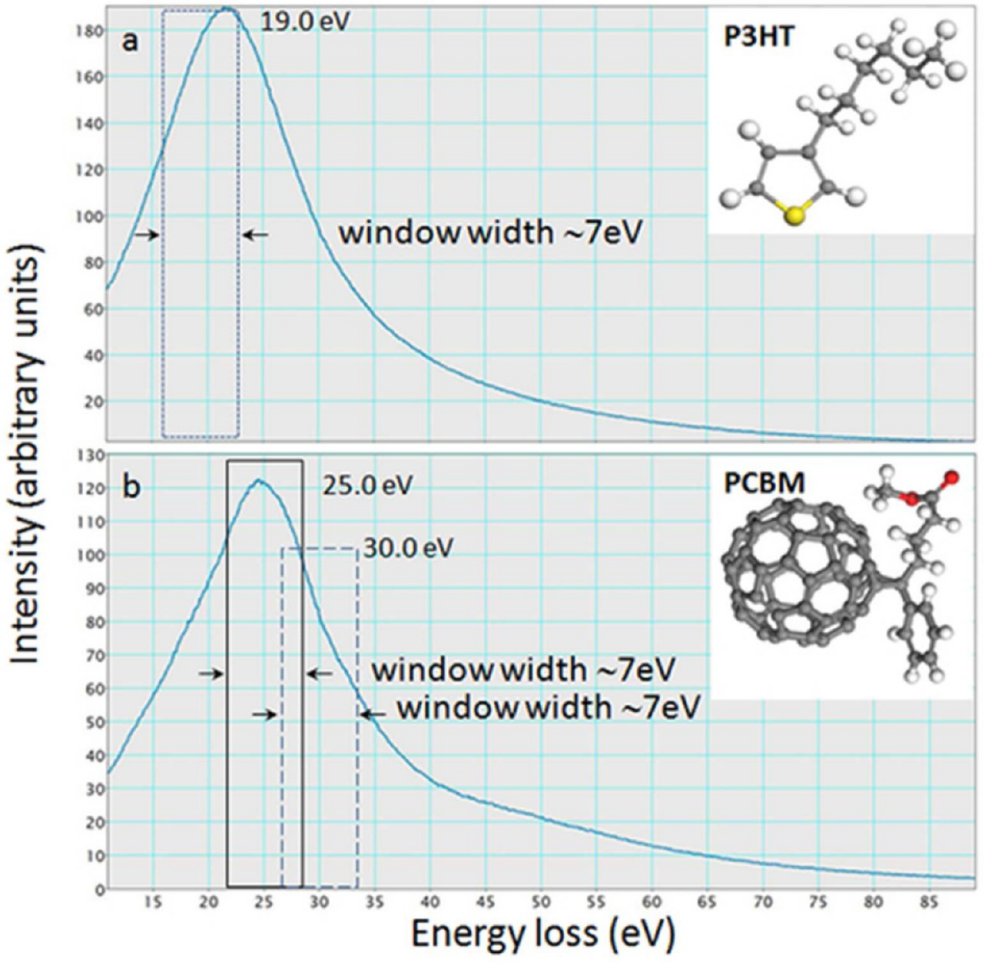

Figure 1. EELS spectra showing plasmon peak positions of neat P3HT and PCBM samples and the respective molecular structures. The plasmon peak for P3HT is located at 21.5 eV, while that of PCBM is at 25.0 eV. The EFTEM images are collected with a window width of 7 eV, as denoted in the spectra at 19, 25, and 30 eV.

provide insight into both exciton separation and charge transport through OPV devices. In this study we used P3HT and PCBM as a model to characterize the nanoscale structure, including the fibrils, which is pertinent to the charge transport in this device. Morphology studies, including investigation of the nanofibril structure in this system, have been reported by several groups by utilizing optical microscopy micrographs with combinations of small- and wide-angle scattering results,[12] conventional bright-field transmission electron microscopy (BFTEM) images, and energy-filtered TEM (EFTEM) images.[14−19] The use of these techniques was recently reviewed by Pfannmöller et al.[20]

TEM is a powerful technique for the characterization of morphology, but the similar mass densities of P3HT and PCBM make the traditional BFTEM technique not feasible and very challenging. The lack of image contrast due to the very similar mass densities of the constituents in this system and/or issues with sample thickness often cause difficulties in determining a conclusive morphology and in the observation of the fibrils. Typically, a poorly contrasted image is observed in conventional BFTEM at the focal point. A common method to enhance the visibility of features with weak contrast is to acquire images under defocused conditions. A series of defocused images can be found in the Supporting Information, Figure S1. For large defocus values, the P3HT fibrils stand out from the background and become well contrasted. However, this enhancement is accompanied by a loss of resolution and a strong delocalization of the image information. This impedes accurate size measurements and the interpretation of the images. Kiel et al.[21] showed that defocused BFTEM images can be misleading and therefore EFTEM images are necessary.[22−24] Drummy et al.[17] presented work using EFTEM images to obtain phase contrast in P3HT/PCBM films. These images showed a better contrast than traditional TEM images. EFTEM shows separate phases in the BHJ films, making it an ideal technique for studying the morphology of OPV devices.

In this work we carry out electron energy loss spectroscopy (EELS) and EFTEM imaging along with selected area electron diffraction (SAED) and X-ray diffraction (XRD) analyses, as well as a cross-section analysis of the device, to provide more precise information on the P3HT/PCBM morphology and P3HT fibril structure. The high-contrast images collected with EFTEM at various loss energies provide distinguishable domains of P3HT, a mixed (P3HT/PCBM) phase, and P3HT fibrils.

2. EXPERIMENTAL SECTION

Details of TEM sample preparation are described in the Supporting Information. In this work, EELS spectra and EFTEM images are collected by a spherical aberration (C_s) corrected TEM microscope

with an in-column OMEGA energy filter (LIBRA 120 PLUS, Zeiss) operating at an accelerating voltage of 120 kV, providing an energy resolution of less than 1.0 eV. The EELS spectra provide three regions of energy loss: zero loss, low loss, and high loss. Figure 1 shows EELS spectra collected in the low-loss region of (a) neat P3HT and (b) PCBM samples with energy loss in the range from 12 to 90 eV. We note that these pronounced energy loss peaks occur as the incoming electrons interact with weakly bound electrons in either the LUMO or HOMO levels, giving rise to a so-called plasmon peak which strongly relates to the material's dielectric constant.[25] We found the plasmon spectra for the neat P3HT and PCBM to have energy losses of 21.5 and 25.0 eV, respectively, which are close to the reported values in the literature.[26]

It is worth mentioning that a switch from spectroscopy to imaging modes is accomplished by collecting electrons via an energy window of specific aperture to create an image on a slow-scan charge-coupled device (CCD) detector (2040 × 2040 pixels). The collection aperture was 600 μm with a slit width of 7 eV. By accounting for the C_s value, collection angle of the spectrometer (β = 10 mrad), width of the energy window (ΔE = 7 eV), and primary electron energy (E = 120 keV), the spatial resolution was calculated to be 1.2 nm.

To find phase distribution information from a cross-section device, a focused ion beam (FIB) sample fabrication technique was used to prepare TEM lamella samples. The TEM lamella preparation is briefly described as follows: A protective layer of Pt was deposited on top of the sample of interest. Two trench-milling areas were created at the edge of the Pt strap with a high current (4 nA) of Ga^+ ions followed by a low current (160 pA) to thin and smooth the sample. The lamella sample was separated by an in situ probe picking system and was mounted on a TEM grid. A fine polishing step with a beam current of about 50 pA was carried out to finally thin the sample to about 50 nm. More information is available in our previous paper on this topic.[27]

3. RESULTS AND DISCUSSION

Figure 2 shows zero-loss (ZL) EFTEM images of P3HT/PCBM (1:1) at two different magnifications. The image

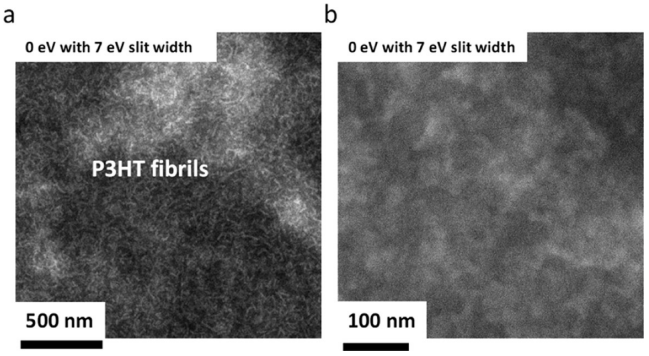

Figure 2. ZL energy-filtered TEM images of P3HT/PCBM (1:1) annealed at 160 °C for 60 min, collected with a ~7 eV window width: (a) image collected at a low magnification showing P3HT fibrils, (b) image collected at high magnification showing a weak-contrast image with indistinguishable features.

collected at zero loss energy (by collecting only elastic electrons) clearly reveals the fibrous morphology at low magnification (500 nm scale bar), as shown in Figure 2a. However, a poorly contrasted image with vague features due to small variations in mass density is observed when the magnification is increased, as shown in Figure 2b. Other groups have also reported that ZL EFTEM of P3HT/PCBM blend exhibits only weak contrast and indistinguishable features.[16,17,26] Similar poor-contrast images were observed in conventional BFTEM at the focal point. Figure 3a shows a low-

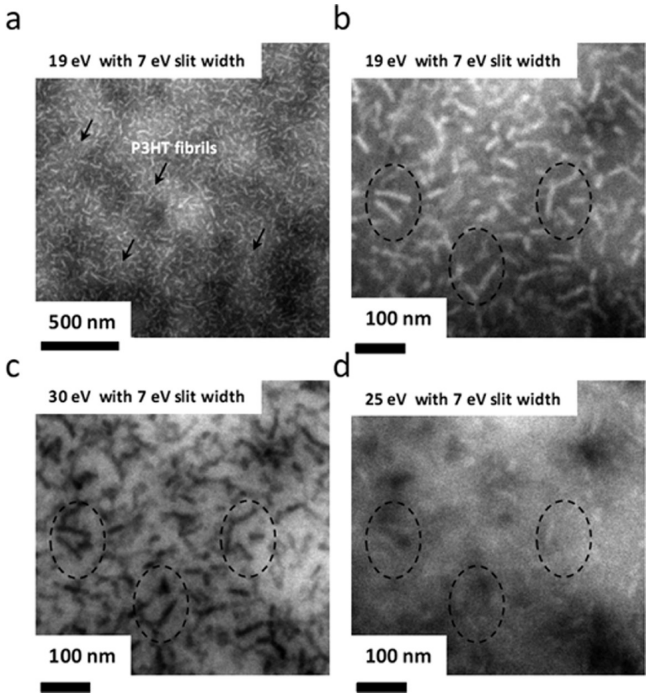

Figure 3. Low-loss EFTEM images collected in a P3HT/PCBM (1:1) sample annealed at 160 °C for 60 min: (a) low-magnification EFTEM image collected at 19 eV energy loss in which the fibrous structure and brighter region contribute to well-distinguished P3HT domains, (b) high-magnification EFTEM image at 19 eV energy loss, (c) EFTEM image collected at 30 eV energy loss, with dark regions corresponding to P3HT fibrils, (d) EFTEM image collected at 25 eV energy loss. All images were collected with the same window width of 7 eV.

magnification micrograph of a 19 eV energy loss EFTEM image collected with a 7 eV slit width on a P3HT/PCBM sample annealed at 160 °C for 60 min. This energy filter creates an image with considerable contrast. A fibrous network is revealed, as evidenced by the white fibrils scattered throughout the image. Unlike those in the image collected with ZL EFTEM, the P3HT fibrils are still observable even at high magnification, as shown in Figure 3b. A high-contrast image is still clearly visible, as collected at an energy loss of 30 eV (Figure 3c). The mixed P3HT/PCBM domains appear bright, while the P3HT fibrils are dark. From Figure 3b,c, it is shown that the fibril-like structure is randomly dispersed and has an overlapping feature, as observed in the 2-dimensional (2-D) micrograph (identified by dotted areas).

Thickness variation can also cause a shift in the brightness of TEM images. This may be responsible for the lighter and darker regions in Figure 3a (light regions marked by arrows). To determine whether thickness variation or the energy loss filter is responsible for these lighter and darker regions throughout the sample, one must capture images at both 19 eV (P3HT bright) and 30 eV (PCBM bright). The use of these energy windows was previously reported by Drummy et al.[17] Figure 3b shows some dark regions (upper right corner) which remain dark at 30 eV (Figure 3c). This confirms that they are due to thickness variations in the sample. However, the fibrils undergo a contrast inversion, showing that they are indeed P3HT fibrils in a PCBM-rich background.

Figure 3d shows a poor-contrast EFTEM image, as collected with 25 eV energy loss. The poor-contrast image is due to the fact that the EELS spectra of the BHJ sample showed a strong

peak at 23.3 eV.[26] The electron intensity in this region is the same for P3HT and PCBM, leading to a poor contrast. Therefore, collecting energy loss at 19 eV (Figure 3b) revealed P3HT fibril-rich domains to appear brighter than PCBM-rich or predominantly mixed P3HT/PCBM regions, while the opposite is true at a 30 eV energy loss. Figure 4 shows EFTEM images of as-prepared (a–c) and annealed (d–f) samples at 160 °C for 20 min. No fibrous network is observed in the as-prepared samples at any energy loss.

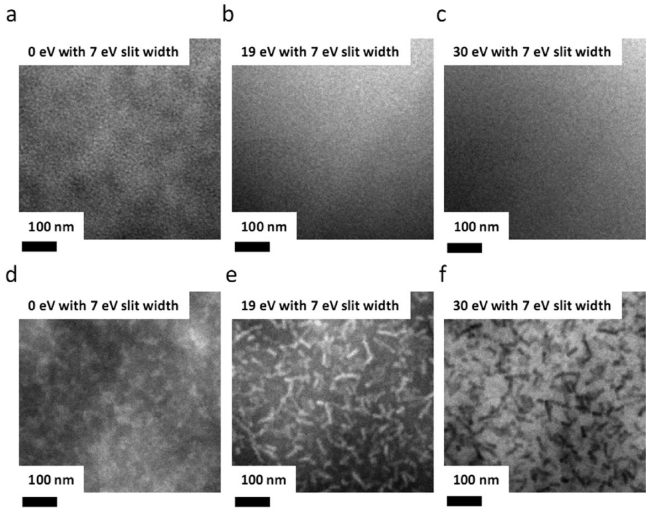

Figure 4. EFTEM images of as-prepared (a–c) and annealed (d–f) samples at 160 °C for 20 min. Note that the images were collected at 0, 19, and 30 eV energy loss, with the same window width at 7 eV.

It is important to note that the samples must be well rinsed to remove any trace of poly(3,4-(ethylenedioxy)thiophene)/poly(styrenesulfonate) (PEDOT/PSS). In Figure S2 (Supporting Information), a small amount of PEDOT/PSS remaining on the sample is clearly observed. AFM analysis was carried out to confirm that the extra material was PEDOT/PSS. Figure 5 is an AFM height image showing the P3HT/PCBM and the remaining PEDOT/PSS (marked by arrows). Please see the Supporting Information (Figures S2 and S3) for more information. It should be noted again that the PEDOT/PSS layer was spin cast for the purpose of detaching the sample from the substrate. The AFM, BFTEM, and EFTEM images in Figures S2 and S3 clearly show that the PEDOT/PSS did not fully dissolve in the deionized water. In practice, after the active layer (P3HT/PCBM) was detached from the substrate, it was allowed to float for 10 min before draining and refilling with fresh deionized water to rinse off the PEDOT/PSS layer. Any remaining PEDOT/PSS was gone after 10 min. AFM analysis shows a root-mean-square (RMS) roughness of ∼1.2 nm and a sample thickness of ∼50 nm.

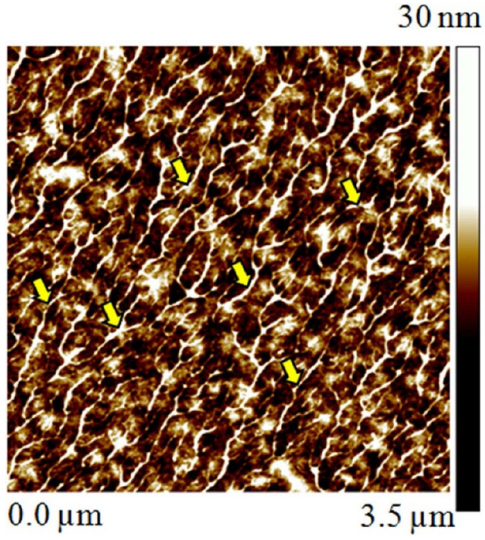

Figure 5. AFM height image of a P3HT/PCBM film showing the remaining PEDOT/PSS material.

Similarly, contrasted images and morphological features corresponding to the pertinent collection energy window were observed on a sample annealed for 20 min, as presented in Figure 4d–f. We determined the fibril's size using Photoshop software on a 2040 × 2040 pixel image and found that the average fibril diameter and lengths are 15 ± 2 and 70 ± 5 nm, respectively. The calculation of the fibril's length is based on the assumption that all fibrils are dispersed parallel to the substrate. The fibril diameter reported by Drummy et al.[17] using Euclidian mapping of EFTEM images is within the same order of magnitude. The fibrils are randomly dispersed with connected and/or overlapped portions, which may cause a major limitation for hole mobility in this semicrystalline polymer. Studies by Savenije et al.[28] showed that the enhanced formation of crystalline P3HT fibrils (demonstrated by more ordered packing of the polymer chains) caused a significant increase in hole mobility after annealing. It is generally understood that the self-organization of P3HT fibrils is caused by both preparation and post thermal treatment.[29,30] As observed, nonconnected and/or overlapped fibrils with lengths of ∼70 nm dispersed in a disordered matrix (mixture of P3HT and PCBM) might cause a low mobility in this semicrystalline polymer. Verilhac et al.[31] proposed that the interconnected structures between the P3HT fiberlike features of high molecular weight (M_w) P3HT increased charge mobility while individually less connected structures of low M_w decreased charge mobility. Similar results were presented by Kline et al.[32] in which the increased carrier mobility and a lower activation energy were obtained from the higher M_w polymer. It is important to note that the morphology, crystallinity, and number of P3HT fiberlike structures were significantly affected by the M_w of the P3HT and sample preparation.[19,31,33] Brinkmann and Rannou[18] showed changes in the morphology of P3HT with respect to M_w using TEM images. The TEM micrographs revealed an obvious "lamellar" structure in P3HT with an M_w of 7.3 kg mol^{-1} and relatively high crystallinity, as characterized by the electron diffraction pattern. When using high M_w P3HT (69.9 kg mol^{-1}), they observed an unclear structure with relatively low crystallinity. Similar observations were also reported by other groups. For example, Ma et al.[34] showed that, in a mixture of P3HT/PCBM, the fibrous network was clearly revealed on an annealed sample with an M_w of 26.2 kg mol^{-1} while no fibrous network was observed on a sample with an M_w of 153.8 kg mol^{-1}. Pfaff et al.[22] presented a sequence of low-energy scanning transmission electron microscopy (STEM) images of P3HT/PCBM blends. They also concluded that the "rodlike" morphology was revealed only on the P3HT with an M_w of 20 kg mol^{-1} whereas "globular structures" were observed on the P3HT with an M_w of 50 kg mol^{-1}. In our study we used a P3HT material (P200) with an M_w of 20–30 kg mol^{-1} and regioregularity of >95%, thereby

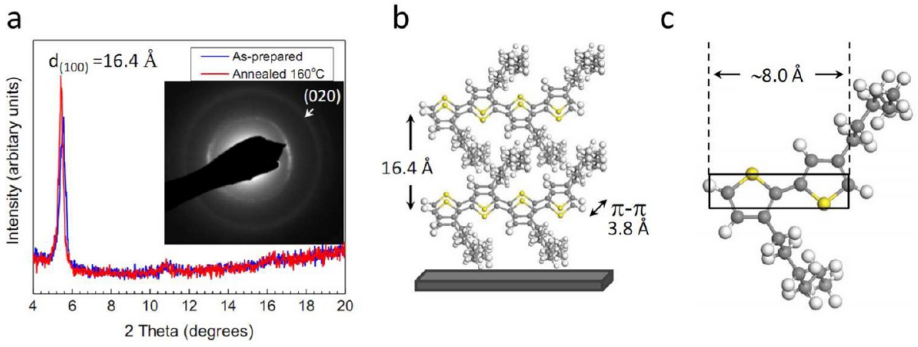

Figure 6. (a) Out-of-plane XRD results of as-prepared samples and samples annealed at 160 °C for 20 min. The inset shows the SAED pattern with (020) reflections of pure P3HT annealed at 160 °C for 20 min, from which the *d* spacing was calculated to be 3.8 Å. (b) Molecular drawing of the ordered polymer chains showing the *d* spacing of 16.4 Å and the $\pi-\pi$ stacking distance of 3.8 Å obtained from XRD and SAED results. (c) Repeating unit of thiophene showing a separation of ~8 Å on the same chain. Note that the yellow spheres indicate S, the gray spheres indicate C, the white spheres indicate H, and the black rectangle indicates an ordered chain.

enabling us to observe the P3HT fibrous structure clearly with EFTEM imaging.

Additionally, the utilization of high M_w polymers toward devices with increased performance and less derivative results was previously reported by several groups[34−36] and recently reviewed by Marrocchi et al.[37] Nicolet et al.[35] showed that, upon annealing, the blend morphology was significantly influenced by the P3HT M_w. Moreover, the facts that the PCBM has a higher solubility in amorphous P3HT regions and an increased phase segregation is obtained upon annealing, as reported previously,[38,39] allow us to observe different phase domains clearly, as shown in Figure 3a. As such, the high-contrast EFTEM image highlights this powerful technique for morphology characterization.

Crystalline orientations of P3HT/PCBM BHJ samples are studied with out-of-plane XRD. Figure 6a shows out-of-plane XRD results on the as-prepared and annealed samples. As shown, the peak intensity at 2θ = 5.3° increases, and small peaks at $2\theta \approx$ 10.6° and 15.9° appear after the samples are annealed, signifying a higher degree of crystallinity. As mentioned earlier, the self-organization of semicrystalline conjugated polymers is significantly enhanced after thermal treatment, resulting in well-ordered polymer chains within a fibrous network. Previous studies using 2-D grazing incidence X-ray diffraction (GIXRD) have shown that the P3HT orientation has a preference for edge-on packing for the high-regioregularity (>91%) P3HT.[40] Chen et al.[41] found a combination of edge-on and face-on configurations upon annealing with crystal sizes of ~23 and ~12 nm, respectively, as calculated by the Scherer formula. By accounting for the regioregularity (>95% in our samples) and preferred chain orientation of the P3HT results, as reported in refs 17, 42, and 43, P3HT ordered chains with an edge-on configuration in the fibrils were determined.

Figure 6b represents a schematic drawing of edge-on packed P3HT in which the spacing between polymer backbones was calculated from the XRD patterns in Figure 6a, showing 16.4 Å interchain spacing perpendicular to the substrate and 3.8 Å $\pi-\pi$ interchain stacking parallel to the substrate. As shown in Figure S4 in the Supporting Information, the in-plane XRD pattern shows a broad peak centered around 2θ = 22.3°, which corresponds to the $\pi-\pi$ distance from the thiophene rings. Since the XRD peak is too broad to use for the $\pi-\pi$ stacking distance calculations, the distance was calculated by SAED using the (020) reflection of P3HT (inset in Figure 6a.). Figure 6c depicts a repeating unit of regioregular P3HT, showing two dimers with a distance of ~8 Å.[44] Using results from the EFTEM images, SAED, and XRD, the number of P3HT repeating units along the fibril structure were determined. There were 18 ± 3 repeating thiophene dimers perpendicular to the fibril length with the quantitative plane alignment, as illustrated in Figure 7. There were approximately 184 layers of $\pi-\pi$ stacking and 9 layers of interchain stacking parallel and perpendicular to the fibril, respectively.

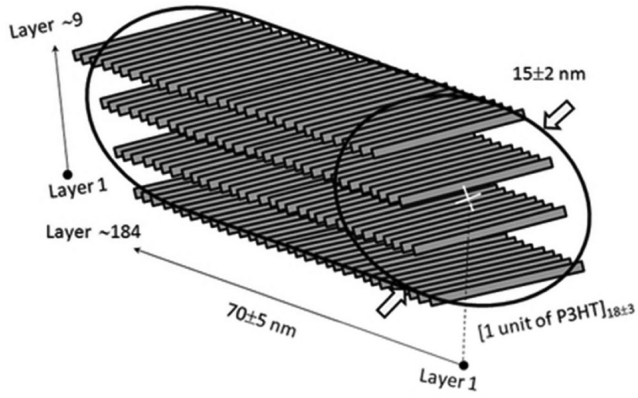

Figure 7. Drawing of a P3HT fibril with a diameter of 15 ± 2 nm and a length of 70 ± 5 nm. The edge-on orientation with ordered chains of P3HT was drawn in the fibril, showing ~184 layers of $\pi-\pi$ stacking and ~9 layers of interchain stacking.

We used EFTEM imaging to further observe the vertical morphology in a conventional BHJ device annealed at 160 °C for 20 min. This device was made using the standard method and was thicker (~160 nm) than the films prepared for the top view (~50 nm). The details are presented in the Supporting Information. Using an FIB sample fabrication technique to prepare TEM lamella samples, as described in our previous work[27] and briefly in the Experimental Section, we were able to observe the vertical phase separation. As mentioned earlier, the conventional BFTEM and STEM images showed a poor phase separation in the cross-section image. Therefore, we collected EFTEM images at various loss energies to observe the cross-section phase separation. Figure 8a shows a schematic drawing of a BHJ device, whereas Figure 8b shows EFTEM images collected at 30 eV with visible P3HT and PCBM phase domains. The EFTEM images collected with respect to

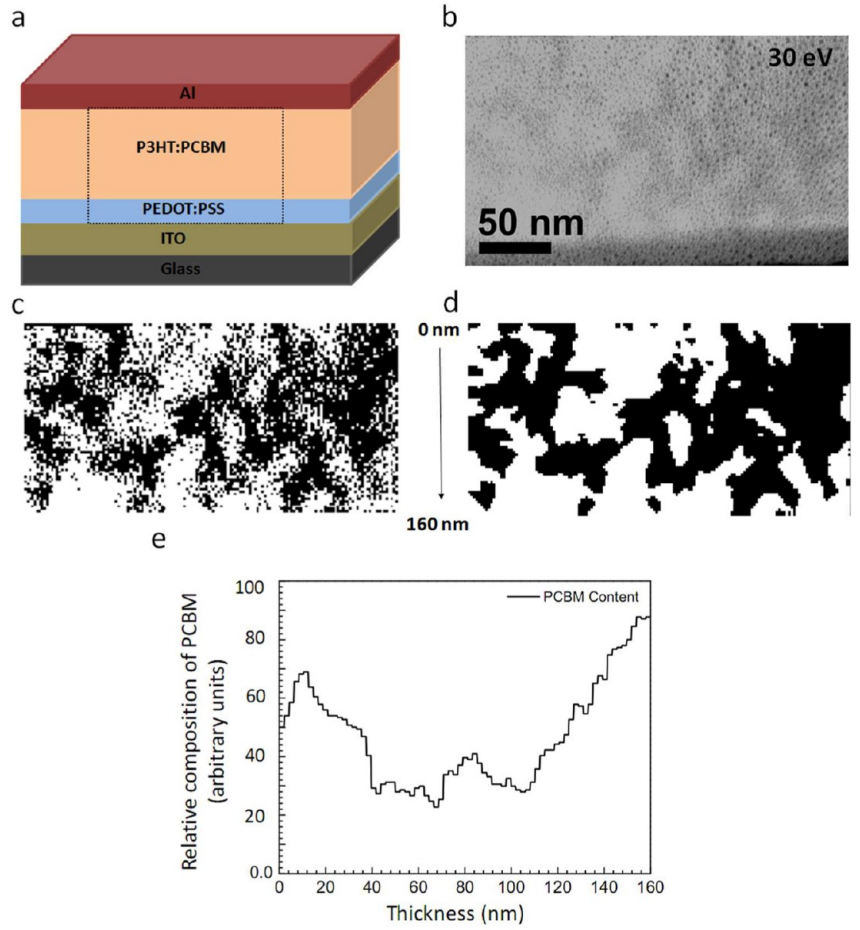

Figure 8. (a) Schematic drawing of a P3HT/PCBM BHJ device, (b) EFTEM image collected at 30 eV energy loss, (c) image digitized by a Matlab program, (d) same image upon averaging the regions, and (e) PCBM distribution over the sample thickness where 0 is the top of the image and 160 nm is the bottom.

different energy losses, i.e., 0 and 19 eV, are presented in the Supporting Information, Figure S5. In the image obtained with 0 eV energy loss, each layer is clearly distinguishable except for the PEDOT/PSS layer. This observation is similar to that made for the BFTEM image, where the low electron densities in polymers give rise to the poor-contrast image. While collecting the image at 19 eV energy loss, we did not observe a fibril-like structure similar to the one visible in Figure 4e. One explanation for this could be that the focused Ga^+ beam, used in creating the cross-section samples, damaged the P3HT fibrils (crystalline region) even at the low current (50 pA) we used while thinning the sample. We note that small dots appearing in the images originated from the redeposition of the sputtered materials during the FIB preparation process. A high-contrast image was observed at 30 eV energy loss (Figure 8b). In the active layer, the brighter area corresponds to PCBM-rich regions while the dark area shows P3HT-rich regions.

To aid in extracting the phase distribution information from the raw EFTEM cross-section images, a combination of filtering and mathematical analyses was used. We began by applying a threshold filter to the image to increase contrast (Figure 8b). As with this contrasted image it was still difficult to discern regions of higher P3HT and PCBM content, we wrote and applied a simple Matlab program. This program first binned every 10 × 10 pixel region, making the small area either black (P3HT) or white (PCBM) depending on the dominant color in the region. Upon running this program, a very grainy black and white image appeared, as illustrated in Figure 8c. To remove any graininess from the dots or noise in the image, we used a smoothing function and created a well-contrasted digital binary image (Figure 8d). It should be noted that these black and white regions in Figure 8d do not represent pure P3HT and pure PCBM regions, but rather regions with high P3HT and PCBM contents. The P3HT/PCBM system could also be represented as a three-phase image (pure P3HT, pure PCBM, and mixed regions), but for simplicity we chose to show a representative binary image. This image can be analyzed to find the relative concentration of PCBM in the device. In this region, we found a composition of 47% P3HT/53% PCBM. This composition very closely matches the expected ratio of 1:1 P3HT/PCBM used in the preparation of the device. We analyzed the PCBM concentration as a function of the thickness of the device (~160 nm) to construct the plot presented in Figure 8e. This plot shows a higher PCBM concentration near the PEDOT/PSS interface, similar to that observed by Kiel et al.[21] This could potentially block holes from reaching the indium tin oxide (ITO) electrode and impede device performance, although connecting P3HT pathways still exist.

4. CONCLUSION

In this paper we presented a quantitative picture of the crystalline order in P3HT fibrils by combining EFTEM images

with XRD and SAED results. Using the plasmon information obtained from EELS spectra, we were able to obtain high-contrast high-resolution TEM images from thin samples. The images revealed a fibrous network of nanocrystalline domains of P3HT dispersed in mixed domains (P3HT and PCBM). The EFTEM images highlighting the random dispersion of P3HT fibrils were obtained by collection with a 19 eV energy loss filter and a 7 eV window. The average fibril was found to be 70 ± 5 nm in length and 15 ± 2 nm in diameter. The out-of-plane XRD results support that the edge-on orientation is favored in this blended system. A quantitative analysis showed that there are 18 ± 3 repeating units of thiophene, ∼184 layers of $\pi-\pi$ stacking, and ∼9 layers of interchain stacking within the fibril-like structure. EFTEM images of the cross-section device were also obtained. These images revealed a nonuniform PCBM distribution with a PCBM-rich region next to the ITO electrode which could lead to a poor device performance due to the mismatch in the energy levels of the materials. To evaluate the P3HT and PCBM distribution with respect to the total device thickness, digitization of a 30 eV EFTEM micrograph was performed with Matlab. Each component, i.e., PCBM and P3HT, was illustrated in white and black pixels, respectively, revealing a 47% P3HT:53% PCBM ratio and the average abundance of these materials.

■ ASSOCIATED CONTENT

Supporting Information

More detailed information about the (i) sample preparation and BFTEM, EFTEM, and AFM images showing the remaining PEDOT/PSS material, (ii) out-of-plane and in-plane XRD analysis, and (iii) EFTEM cross-section images collected at various energy losses. This material is available free of charge via the Internet at http://pubs.acs.org.

■ AUTHOR INFORMATION

Corresponding Author

*E-mail: Ismat@udel.edu. Phone: 302-831-1618. Fax: 302-831-4545.

Notes

The authors declare no competing financial interest.

■ ACKNOWLEDGMENTS

This work was supported by the U.S. Department of State under Phase 4 of the Pakistan-U.S. Science and Technology Cooperation Program (Grant PGA-P210859). N.R. acknowledges the Thai Government for full support with a financial grant for his Ph.D. program.

■ REFERENCES

(1) Li, G.; Shrotriya, V.; Huang, J.; Yao, Y.; Moriarty, T.; Emery, K.; Yang, Y. High-Efficiency Solution Processable Polymer Photovoltaic Cells by Self-Organization of Polymer Blends. *Nat. Mater.* **2005**, *4*, 864−868.

(2) Shrotriya, V. Organic Photovoltaics: Polymer Power. *Nat. Photonics* **2009**, *3*, 447−449.

(3) He, Z.; Zhong, C.; Su, S.; Xu, M.; Wu, H.; Cao, Y. Enhanced Power-Conversion Efficiency in Polymer Solar Cells Using an Inverted Device Structure. *Nat. Photonics* **2012**, *6*, 591−595.

(4) Yu, G.; Gao, J.; Hummelen, J. C.; Wudl, F.; Heeger, A. J. Polymer Photovoltaic Cells: Enhanced Efficiencies via a Network of Internal Donor-Acceptor Heterojunctions. *Science* **1995**, *270*, 1789−1791.

(5) Clarke, T. M.; Durrant, J. R. Charge Photogeneration in Organic Solar Cells. *Chem. Rev.* **2010**, *110*, 6736−6767.

(6) Choulis, S. A.; Kim, Y.; Nelson, J.; Bradley, D. D. C.; Giles, M.; Shkunov, M.; McCulloch, I. High Ambipolar and Balanced Carrier Mobility in Regioregular Poly(3-hexylthiophene). *Appl. Phys. Lett.* **2004**, *85*, 3890.

(7) Goh, C.; Kline, R. J.; McGehee, M. D.; Kadnikova, E. N.; Fréchet, J. M. J. Molecular-Weight-Dependent Mobilities in Regioregular Poly(3-hexyl-thiophene) Diodes. *Appl. Phys. Lett.* **2005**, *86*, 122110.

(8) Lan, Y.-K.; Yang, C. H.; Yang, H.-C. Theoretical Investigations of Electronic Structure and Charge Transport Properties in Polythiophene-Based Organic Field-Effect Transistors. *Polym. Int.* **2010**, *59*, 16−21.

(9) Lan, Y.-K.; Huang, C.-I. Charge Mobility and Transport Behavior in the Ordered and Disordered States of the Regioregular Poly(3-hexylthiophene). *J. Phys. Chem. B* **2009**, *113*, 14555−14564.

(10) Kevin, M.; Coakley, K. M.; Srinivasan, B. S.; Ziebarth, J. M.; Goh, C.; Liu, Y.; McGehee, M. D. Enhanced Hole Mobility in Regioregular Polythiophene Infiltrated in Straight Nanopores. *Adv. Funct. Mater.* **2005**, *15*, 1927−1932.

(11) Kohn, P.; Rong, Z.; Scherer, K. H.; Sepe, A.; Sommer, M.; Müller-Buschbaum, P.; Friend, R. H.; Steiner, U.; Hüttner, S. Crystallization-Induced 10-nm Structure Formation in P3HT/PCBM Blends. *Macromolecules* **2013**, *46*, 4002−4013.

(12) Ruderer, M. a.; Guo, S.; Meier, R.; Chiang, H.-Y.; Körstgens, V.; Wiedersich, J.; Perlich, J.; Roth, S. V.; Müller-Buschbaum, P. Solvent-Induced Morphology in Polymer-Based Systems for Organic Photovoltaics. *Adv. Funct. Mater.* **2011**, *21*, 3382−3391.

(13) Guo, S.; Ruderer, M. A.; Rawolle, M.; Körstgens, V.; Birkenstock, C.; Perlich, J.; Müller-Buschbaum, P. Evolution of Lateral Structures during the Functional Stack Build-Up of P3HT:PCBM-Based Bulk Heterojunction Solar Cells. *ACS Appl. Mater. Interfaces* **2013**, *5*, 8581−8590.

(14) Yang, X.; Loos, J.; Veenstra, S. C.; Verhees, W. J. H.; Wienk, M. M.; Kroon, J. M.; Michels, M. A. J.; Janssen, R. A. J. Nanoscale Morphology of High-Performance Polymer Solar Cells. *Nano Lett.* **2005**, *5*, 579−583.

(15) Van Bavel, S. S.; Bärenklau, M.; de With, G.; Hoppe, H.; Loos, J. P3HT/PCBM Bulk Heterojunction Solar Cells: Impact of Blend Composition and 3D Morphology on Device Performance. *Adv. Funct. Mater.* **2010**, *20*, 1458−1463.

(16) Pfannmöller, M.; Flügge, H.; Benner, G.; Wacker, I.; Sommer, C.; Hanselmann, M.; Schmale, S.; Schmidt, H.; Hamprecht, F. A.; Rabe, T.; Kowalsky, W.; Schröder, R. R. Visualizing a Homogeneous Blend in Bulk Heterojunction Polymer Solar Cells by Analytical Electron Microscopy. *Nano Lett.* **2011**, *11*, 3099−3107.

(17) Drummy, L. F.; Davis, R. J.; Moore, D. L.; Durstock, M.; Vaia, R. A.; Hsu, J. W. P. Molecular-Scale and Nanoscale Morphology of P3HT:PCBM Bulk Heterojunctions: Energy-Filtered TEM and Low-Dose HREM. *Chem. Mater.* **2011**, *23*, 907−912.

(18) Brinkmann, M.; Rannou, P. Effect of Molecular Weight on the Structure and Morphology of Oriented Thin Films of Regioregular Poly(3-hexylthiophene) Grown by Directional Epitaxial Solidification. *Adv. Funct. Mater.* **2007**, *17*, 101−108.

(19) Brinkmann, M.; Rannou, P. Molecular Weight Dependence of Chain Packing and Semicrystalline Structure in Oriented Films of Regioregular Poly(3-hexylthiophene) Revealed by High-Resolution Transmission Electron Microscopy. *Macromolecules* **2009**, *42*, 1125−1130.

(20) Pfannmöller, M.; Kowalsky, W.; Schröder, R. R. Visualizing Physical, Electronic, and Optical Properties of Organic Photovoltaic Cells. *Energy Environ. Sci.* **2013**, *6*, 2871.

(21) Kiel, J. W.; Kirby, B. J.; Majkrzak, C. F.; Maranville, B. B.; Mackay, M. E. Nanoparticle Concentration Profile in Polymer-Based Solar Cells. *Soft Matter* **2010**, *6*, 641.

(22) Pfaff, M.; Klein, M. F. G.; Müller, E.; Müller, P.; Colsmann, A.; Lemmer, U.; Gerthsen, D. Nanomorphology of P3HT:PCBM-Based Absorber Layers of Organic Solar Cells after Different Processing Conditions Analyzed by Low-Energy Scanning Transmission Electron Microscopy. *Microsc. Microanal.* **2012**, *18*, 1380−1388.

(23) Sawyer, L. C.; Grubb, D. T. *Polymer Microscopy*, 2nd ed.; Chapman and Hall: London, 1996.
(24) Michler, G. H. *Electron Microscopy of Polymers*; Springer: Berlin, 2008.
(25) Williams, D. B.; Carter, C. B. *Transmission Electron Microscopy Part 4: Spectrometry*, 2nd ed.; Springer: New York, 2009.
(26) Herzing, A. A.; Richter, L. J.; Anderson, I. M. 3D Nanoscale Characterization of Thin-Film Organic Photovoltaic Device Structures via Spectroscopic Contrast in the TEM. *J. Phys. Chem. C* **2010**, *114*, 17501−17508.
(27) Rujisamphan, N.; Deng, F.; Murray, R. E.; Ni, C.; Ismat Shah, S. Focused Ion Beam Assisted Investigations of Al Interface in Polythiophene:Fullerene Solar Cells. *Sol. Energy Mater. Sol. Cells* **2013**, *109*, 56−62.
(28) Savenije, T. J.; Kroeze, J. E.; Yang, X.; Loos, J. The Effect of Thermal Treatment on the Morphology and Charge Carrier Dynamics in a Polythiophene-Fullerene Bulk Heterojunction. *Adv. Funct. Mater.* **2005**, *15*, 1260−1266.
(29) Ma, W.; Yang, C.; Gong, X.; Lee, K.; Heeger, A. J. Thermally Stable, Efficient Polymer Solar Cells with Nanoscale Control of the Interpenetrating Network Morphology. *Adv. Funct. Mater.* **2005**, *15*, 1617−1622.
(30) Kim, Y.; Cook, S.; Tuladhar, S. M.; Choulis, S. A.; Nelson, J.; Durrant, J. R.; Bradley, D. D. C.; Giles, M.; McCulloch, I.; Ha, C.-S.; Ree, M. A Strong Regioregularity Effect in Self-Organizing Conjugated Polymer Films and High-Efficiency Polythiophene:Fullerene Solar Cells. *Nat. Mater.* **2006**, *5*, 197−203.
(31) Verilhac, J.-M.; LeBlevennec, G.; Djurado, D.; Rieutord, F.; Chouiki, M.; Travers, J.-P.; Pron, A. Effect of Macromolecular Parameters and Processing Conditions on Supramolecular Organisation, Morphology and Electrical Transport Properties in Thin Layers of Regioregular Poly(3-hexylthiophene). *Synth. Met.* **2006**, *156*, 815−823.
(32) Kline, R. J.; Mcgehee, M. D.; Kadnikova, E. N.; Liu, J.; Fre, J. M. J.; Toney, M. F. Dependence of Regioregular Poly(3-hexylthiophene) Film Morphology and Field-Effect Mobility on Molecular Weight. *Macromolecules* **2005**, *38*, 3312−3319.
(33) Park, J. H.; Kim, J. S.; Lee, J. H.; Lee, W. H.; Cho, K. Effect of Annealing Solvent Solubility on the Performance of Poly(3-hexylthiophene)/Methanofullerene Solar Cells. *J. Phys. Chem. C* **2009**, *113*, 17579−17584.
(34) Ma, W.; Kim, J. Y.; Lee, K.; Heeger, A. J. Effect of the Molecular Weight of Poly(3-hexylthiophene) on the Morphology and Performance of Polymer Bulk Heterojunction Solar Cells. *Macromol. Rapid Commun.* **2007**, *28*, 1776−1780.
(35) Nicolet, C.; Deribew, D.; Renaud, C.; Fleury, G.; Brochon, C.; Cloutet, E.; Vignau, L.; Wantz, G.; Cramail, H.; Geoghegan, M.; Hadziioannou, G. Optimization of the Bulk Heterojunction Composition for Enhanced Photovoltaic Properties: Correlation between the Molecular Weight of the Semiconducting Polymer and Device Performance. *J. Phys. Chem. B* **2011**, *115*, 12717−12727.
(36) Li, L.; Lu, G.; Yang, X. Improving Performance of Polymer Photovoltaic Devices Using an Annealing-Free Approach via Construction of Ordered Aggregates in Solution. *J. Mater. Chem.* **2008**, *18*, 1984.
(37) Marrocchi, A.; Lanari, D.; Facchetti, A.; Vaccaro, L. Poly(3-hexylthiophene): Synthetic Methodologies and Properties in Bulk Heterojunction Solar Cells. *Energy Environ. Sci.* **2012**, *5*, 8457.
(38) Chen, D.; Liu, F.; Wang, C.; Nakahara, A.; Russell, T. P. Bulk Heterojunction Photovoltaic Active Layers via Bilayer. *Nano Lett.* **2011**, 2071−2078.
(39) Watts, B.; Belcher, W. J.; Thomsen, L.; Ade, H.; Dastoor, P. C. A Quantitative Study of PCBM Diffusion during Annealing of P3HT:PCBM Blend Films. *Macromolecules* **2009**, *42*, 8392−8397.
(40) Sirringhaus, H.; Brown, P. J.; Friend, R. H.; Nielsen, M. M.; Bechgaard, K.; Langeveld-Voss, B. M. W.; Spiering, A. J. H.; Janssen, R. A. J.; Meijer, E. W.; Herwig, P.; de Leeuw, D. M. Two-Dimensional Charge Transport in Self-Organized, High-Mobility Conjugated Polymers. *Nature* **1999**, *401*, 685−688.
(41) Chen, D.; Nakahara, A.; Wei, D.; Nordlund, D.; Russell, T. P. P3HT/PCBM Bulk Heterojunction Organic Photovoltaics: Correlating Efficiency and Morphology. *Nano Lett.* **2011**, *11*, 561−567.
(42) Ewbank, R. P. C.; Laird, R. D. M. In *Organic Photovoltaics—Materials, Device Physics, and Manufacturing Technologies*; Brabec, C. J., Dyakonov, V., Scherf, U., Eds.; John Wiley & Sons: Weinheim, Germany, 2008.
(43) Ihn, K. J.; Moulton, J.; Smith, P. Whiskers of Poly(3-alkylthiophene)s. *J. Polym. Sci., Part B: Polym. Phys.* **1993**, *31*, 735−742.
(44) Cheung, D. L.; McMahon, D. P.; Troisi, A. Computational Study of the Structure and Charge-Transfer Parameters in Low-Molecular-Mass P3HT. *J. Phys. Chem. B* **2009**, *113*, 9393−9401.